JGP Journal of General Physiology

RESEARCH ARTICLE

Bile acids inhibit human purinergic receptor P2X4 in a heterologous expression system

Alexandr V. Ilyaskin, Florian Sure, Viatcheslav Nesterov, Silke Haerteis, and Christoph Korbmacher

We recently demonstrated that bile acids, especially tauro-deoxycholic acid (t-DCA), modify the function of the acid-sensing ion channel ASIC1a and other members of the epithelial sodium channel (ENaC)/degenerin (DEG) ion channel family. Surprisingly, ASIC1 shares a high degree of structural similarity with the purinergic receptor P2X4, a nonselective cation channel transiently activated by ATP. P2X4 is abundantly expressed in the apical membrane of bile duct epithelial cells and is therefore exposed to bile acids under physiological conditions. Here, we hypothesize that P2X4 may also be modulated by bile acids and investigate whether t-DCA and other common bile acids affect human P2X4 heterologously expressed in *Xenopus laevis* oocytes. We find that application of either t-DCA or unconjugated deoxycholic acid (DCA; 250 µM) causes a strong reduction (~70%) of ATP-activated P2X4-mediated whole-cell currents. The inhibitory effect of 250 µM tauro-chenodeoxycholic acid is less pronounced (~30%), and 250 µM chenodeoxycholic acid, cholic acid, or tauro-cholic acid did not significantly alter P2X4-mediated currents. t-DCA inhibits P2X4 in a concentration-dependent manner by reducing the efficacy of ATP without significantly changing its affinity. Single-channel patch-clamp recordings provide evidence that t-DCA inhibits P2X4 by stabilizing the channel's closed state. Using site-directed mutagenesis, we identifiy several amino acid residues within the transmembrane domains of P2X4 that are critically involved in mediating the inhibitory effect of t-DCA on P2X4. Importantly, a W46A mutation converts the inhibitory effect of t-DCA into a stimulatory effect. We conclude that t-DCA directly interacts with P2X4 and decreases ATP-activated P2X4 currents by stabilizing the closed conformation of the channel.

Introduction

The human P2X receptor family of ATP-gated nonselective cation channels consists of seven members (P2X1–7; North, 2002). P2X receptors are critically involved in ATP-mediated purinergic auto-/paracrine cell signaling and play an important role in various physiological processes, including renal autoregulation, intestinal neurotransmission, and the regulation of vascular tone (Corriden and Insel, 2010; Kaczmarek-Hájek et al., 2012). Upon ATP binding, P2X channels undergo a conformational change, resulting in the opening of an ion permeation pathway (Khakh and North, 2006). This leads to Na^+ and, most importantly, Ca^{2+} influx, which results in a wide range of cellular responses.

Recent evidence suggests that P2X-mediated purinergic signaling contributes to liver and biliary homeostasis (Fausther et al., 2012). Among the members of the P2X family, the P2X4 receptor has the most prominent expression in liver and bile ducts (Doctor et al., 2005; Fausther et al., 2012; Tabibian et al., 2013). Moreover, the P2X4 receptor was found to be abundantly expressed in the apical membrane of intrahepatic bile duct epithelial cells, the cholangiocytes (Doctor et al., 2005). Thus, bile acids may directly interact with P2X4 in bile ducts under physiological conditions.

Several allosteric modulators of P2X4 have been identified, i.e., protons, zinc ions, ethanol, neurosteroids, and the antiparasitic drug ivermectin (IVM; Coddou et al., 2011a,b; Habermacher et al., 2016). For the lipophilic compound IVM, a putative binding site has been described within the transmembrane domains of P2X4 at the intersubunit protein–membrane interface (Silberberg et al., 2007; Popova et al., 2013; Latapiat et al., 2017). The amphiphilic bile acids are also membrane active substances, which may incorporate into the membrane and interact with the transmembrane domain of P2X4. Recently, we have demonstrated that bile acids can modify the function of the acid-sensing ion channel (ASIC) 1a (ASIC1a) and other members of the epithelial sodium channel (ENaC)/degenerin (DEG) ion channel family (Ilyaskin et al., 2016, 2017, 2018).

Institut für Zelluläre und Molekulare Physiologie, Friedrich-Alexander-Universität Erlangen-Nürnberg, Erlangen, Germany.

Correspondence to Christoph Korbmacher: christoph.korbmacher@fau.de; Alexandr V. Ilyaskin: alexandr.ilyaskin@fau.de; Silke Haerteis' present address is Lehrstuhl für Molekulare und Zelluläre Anatomie, Universität Regensburg, Regensburg, Germany.

Moreover, we described a putative bile acid binding region at the intersubunit interface within the transmembrane domain of ENaC/DEG channels (so-called degenerin region). Thus, the proposed bile acid binding site of ENaC/DEG channels and the putative IVM binding site of P2X4 are both thought to involve transmembrane domains between adjacent channel subunits.

ASICs and P2X receptors have no significant amino acid sequence homology. However, a comparison of the *Danio rerio* P2X4.1 crystal structure (67% sequence similarity with human P2X4) with that of ASIC1 revealed a high degree of similarity in topology and architecture of the two channels (Gonzales et al., 2009; Kawate et al., 2009; Hattori and Gouaux, 2012). Similar to ASIC1, P2X4 forms homotrimeric channels and the structure of individual P2X4 subunits is characterized by a large extracellular domain, short intracellular N- and C-termini, and two transmembrane helices (TM1 and TM2).

We hypothesized that due to their structural similarities ASIC1 and P2X4 may share some common mechanisms of channel regulation and channel gating. The aim of the present study was to investigate whether bile acids affect ATP-activated P2X4-mediated currents.

Materials and methods

Chemicals

Sodium salt of cholic (CA) and tauro-cholic acid (t-CA), deoxycholic (DCA) and tauro-deoxycholic acid (t-DCA), chenodeoxycholic (CDCA) and tauro-chenodeoxycholic acid (t-CDCA), as well as ATP dipotassium salt were purchased from Sigma-Aldrich.

Plasmids

Genomic product (full-length cDNA encoding human P2X4; I.M.A.G.E.Clone ID 5216449; Lennon et al., 1996) was provided by Source BioScience UK Limited. It was subcloned into the pTLN vector (Lorenz et al., 1996). Linearized plasmids were used as templates for complementary RNA (cRNA) synthesis using T7 RNA polymerases (mMessage mMachine; Ambion). Single-point mutations (Y42A, W46A, W50A, W51A, D331A, M336A) were introduced in P2X4 using the QuikChange II site-directed mutagenesis kit (Stratagene). Sequences were confirmed by sequence analysis (LGC Genomics). An antisense phosphothioat-oligoDNA against *Xenopus* Cx38 was synthesized by biomers.net GmbH.

Isolation of oocytes and two-electrode voltage-clamp experiments

Isolation of oocytes and two-electrode voltage-clamp experiments were performed essentially as described previously (Diakov and Korbmacher, 2004; Haerteis et al., 2009; Diakov et al., 2010; Ilyaskin et al., 2016, 2017, 2018). Defolliculated stage V–VI oocytes were collected from ovarian lobes of female *Xenopus laevis* with approval of the animal welfare officer of the University of Erlangen-Nürnberg, in accordance with the principles of German legislation and under state veterinary health inspectorate governance. Animals were anesthetized in 0.2% ethyl 3-aminobenzoate methanesulfonate (MS-222; Sigma-Aldrich), and ovarian lobes were obtained by a small abdominal incision. Oocytes were injected with 2–5 ng cRNA for WT or mutant human P2X4. To suppress the expression and possible interference of endogenous connexin 38 (Cx38) hemichannels, an established approach (Ebihara, 1996; Bahima et al., 2006) was used. 3 ng of the antisense phosphothioat-oligoDNA corresponding to nucleotides −5 to +25 of the coding region of Cx38 (5′-GCTTTAGTAATTCCCATCCTGCCATGTTTC-3′) was routinely co-injected into the oocytes together with P2X4 cRNA. Oocytes injected only with antisense DNA against Cx38 were used as control oocytes. To minimize P2X4-mediated Na^+ influx, injected oocytes were kept in a low-sodium solution (ND9; in mM: 9 NaCl, 2 KCl, 87 N-methyl-D-glutamine-Cl, 1.8 $CaCl_2$, 1 $MgSO_4$, and 5 HEPES, pH 7.4 adjusted with Tris) supplemented with 100 units/ml sodium penicillin and 100 µg/ml streptomycin sulfate to inhibit bacterial growth. Oocytes were studied 48 h after cRNA injection. To prevent an activation of endogenous calcium–activated chloride channels by P2X4-mediated calcium influx, Ca^{2+}-free ND96 solution was routinely used as bath solution (in mM: 96 NaCl, 4 KCl, 1 EGTA, 1 $MgCl_2$, and 10 HEPES, pH 7.4 adjusted with Tris). Bath solution exchanges with a gravity-fed system were controlled by a magnetic valve system (ALA BPS-8) in combination with a TIB14 interface (HEKA). An individual oocyte was placed in an experimental chamber with a narrow flow channel (length: 45 mm; height: 3 mm; width: 3 mm) with a U-shaped cross-section of ∼8 mm^2. The oocyte was positioned in the experimental chamber close to the site of solution inflow and was held in place by the impaling microelectrodes. To achieve rapid and reproducible solution exchanges at the oocyte, the perfusion rate was carefully adjusted for each experimental solution to ∼10 ml/min, resulting in a flow velocity of ∼20 mm/s. The flow channel drained into a reservoir (2 cm × 1 cm) from which the solution was continuously removed via a suction tube. The suction tube was adjusted to maintain the fluid level in the flow channel at ∼2 mm. Whole-cell current recordings started typically within 10 s after impalement of an oocyte with microelectrodes. Oocytes were clamped at a holding potential of −60 mV using an OC-725C amplifier (Warner Instruments) connected by a LIH-1600 (HEKA) to a personal computer. Pulse 8.78 software (HEKA) was used for data acquisition.

Single-channel recordings in outside-out patches

Single-channel recordings in outside-out membrane patches of P2X4-expressing oocytes were performed 48 h after injection of 2 or 5 ng WT P2X4 cRNA using a conventional patch-clamp technique essentially as described previously (Diakov and Korbmacher, 2004; Lefèvre et al., 2014; Ilyaskin et al., 2016, 2017, 2018). Patch pipettes were pulled from borosilicate glass capillaries and had a tip diameter of ∼1–1.5 µm after fire polishing. Pipettes were filled with K-gluconate pipette solution (in mM: 90 K-gluconate, 5 NaCl, 2 EGTA, and 10 HEPES, pH 7.2 adjusted with Tris). The pipette solution contained no ATP to avoid a possible exposure of P2X4 to ATP during seal formation. Ca^{2+}-containing ND96 solution was used as bath solution (in mM: 96 NaCl, 4 KCl, 1 $CaCl_2$, 1 $MgCl_2$, and 10 HEPES, pH 7.4 adjusted with Tris). In this bath solution, the pipette resistance averaged ∼7–9 MΩ.

The holding potential was set to −70 mV. Using a 3-M KCl flowing boundary electrode, the liquid junction potential occurring at the pipette/ND96 bath junction was measured to be 12 mV (bath positive; Lefèvre et al., 2014). Thus, at a holding potential of −70 mV, the effective trans-patch potential was −82 mV. This value is close to the calculated equilibrium potential of Cl^- (E_{Cl^-} = −77.4 mV) and K^+ (E_{K^+} = −79.4 mV) under our experimental conditions. Experiments were performed at room temperature using an elongated flow chamber continuously perfused with bath solution. To change from one bath solution to another a conventional gravity-fed system controlled by a magnetic valve system (ALA BPS-8) was used in combination with a TIB14 interface (HEKA). The manifold receiving the different experimental bath solutions and the small-diameter tube (internal tube diameter: 1 mm) connecting the manifold to the experimental chamber had a dead volume of ∼50 µl. At a flow rate of ∼1 ml/min, the estimated exchange time of the dead volume was ∼3 s. Thus, when switching from one solution to another solution, the fluid exchange at the patch occurred with a delay of ∼3 s. Indeed, this estimated delay time is consistent with previously published data obtained with the same experimental system (Ilyaskin et al., 2017). Re-analysis of the data from this latter study revealed a rather constant delay time of 2.8 ± 0.3 s (n = 12) between switching the magnetic valve to a low-pH solution and the onset of proton-activated ASIC1-mediated currents. The excised patch at the tip of the pipette was positioned in the chamber in close proximity to the opening of the inflow tube in the center of the fluid flow, which had a velocity of ∼20 mm/s, ensuring a reasonably rapid solution exchange at the patch after the delay caused by the dead volume. Single-channel current data were initially filtered at 2 kHz and sampled at 6 kHz. The current traces were digitally refiltered at 400 Hz using Gaussian filtering to resolve single-channel events. Filtering at a higher frequency was not used to avoid detection of false-positive events. The apparent number of active channels in a patch was determined by visual inspection of the current traces. Single-channel data were analyzed using the program "Nest-o-Patch" written by Dr. V. Nesterov. Binned amplitude histograms were generated to determine channel closed and open levels and to estimate the single-channel current amplitude (i). In patches with only one active channel, open probability (P_o) was estimated from the time integral of current exceeding the channel closed level divided by the product of i and total duration of the analyzed portion of the current trace. Alternatively, dwell-time data generated for the analysis of single-channel kinetics were used to estimate P_o according to the following equation: $P_o = t_{open}/(t_{open} + t_{close})$, where t_{open} is the sum of the durations of all channel openings and t_{close} is the sum of the durations of all channel closures. Dwell times were determined by detecting individual channel opening and closing events using a half-amplitude threshold crossing algorithm. With Gaussian filtering at 400-Hz cutoff frequency the minimal duration of a detectable event was ∼0.45 ms. Durations of channel open and closed times from similar recordings were summarized in a joint events table. The latter was used to calculate mean channel open and closed times and to generate dwell-time histograms as described by Sigworth and Sine (1987) for the analysis of open-time and closed-time constants. Dwell-time histograms were fitted with exponential functions using R environment for statistical computing version 3.5.2 (R Foundation for Statistical Computing; www.R-project.org).

Homology models of human P2X4 and molecular docking approach

The homology models of human P2X4 were built using the MODELLER 9.12 package (Sali and Blundell, 1993; Webb and Sali, 2014) and the crystal structure of *D. rerio* P2X4.1 in its closed state (PDB accession no. 4DW0) or open state (PDB accession no. 4DW1) as a template (Hattori and Gouaux, 2012). Putative t-DCA binding site in the transmembrane domains of human P2X4 in the channel closed state was predicted using the molecular docking software AutoDock Vina (Trott and Olson, 2010). The structure of t-DCA was extracted from ZINC version 12 database (ZINC ID: ZINC04282168; Irwin and Shoichet, 2005). The t-DCA structure was prepared for docking by defining the rotatable bonds using AutoDockTools 1.5.6 (Sanner, 1999; Morris et al., 2009). The grid box defining the docking boundaries was assigned using AutoDockTools 1.5.6. Ten runs of the program were performed with 10 binding modes generated per run, giving a total number of 100 docked t-DCA modes.

Statistical methods

Data are presented as means ± SEMs and individual data points. Statistical significance was assessed by unpaired Student's t test or the one-way ANOVA with Bonferroni post hoc test. N indicates the number of different batches of oocytes and n the number of individual oocytes studied. Data of concentration-dependent P2X4 inhibition by t-DCA and ATP-dependent stimulation of P2X4 were normalized as indicated in the corresponding figures and were fitted using the following equation:

$$Q_{norm} = Q_{norm,min} + \left(Q_{norm,max} - Q_{norm,min}\right) \Big/ \left[1 + \left(C_{50}/C\right)^{Hill}\right], \quad (1)$$

where Q_{norm} is the actual normalized current integral, $Q_{norm,min}$ is the minimal normalized current integral, $Q_{norm,max}$ is the maximal normalized current integral, C is the concentration of t-DCA or ATP, C_{50} is the t-DCA or ATP concentration at which the half-maximal response occurs, and $Hill$ is the Hill coefficient.

The initial linear phase of an individual ATP-activated P2X4-mediated ensemble current response was fitted with a linear function:

$$I_{P2X4} = s_{act}t, \quad (2)$$

where I_{P2X4} is the ATP-activated P2X4-mediated ensemble current, s_{act} is the slope of the linearly increasing current, and t is time.

The spontaneous decrease in the P2X4-mediated ensemble current was fitted with an exponential decay function:

$$I_{P2X4} = I_{P2X4,max}e^{-\frac{t}{\tau_{inact}}}, \quad (3)$$

where I_{P2X4} is the ATP-activated P2X4-mediated ensemble current, $I_{P2X4,max}$ is the maximal ATP-activated P2X4-mediated ensemble current, τ_{inact} is the characteristic time constant of

spontaneous current inactivation, and t is time. Statistical analysis was performed using GraphPad Prism 5.04.

Results

Modulation of human P2X4 by bile acids

We have previously shown that t-DCA has a strong stimulatory effect on human ENaC in its αβγ and δβγ subunit configuration, on human bile acid–sensitive ion channel (BASIC) and on human ASIC1a (Ilyaskin et al., 2016, 2017, 2018). Therefore, we investigated the effect of t-DCA on human P2X4 heterologously expressed in *X. laevis* oocytes. P2X4-mediated whole-cell currents were measured using the two-electrode voltage-clamp technique. As shown in the representative current trace in Fig. 1 A, repeated applications of ATP (10 µM for 10 s with 2-min intervals) elicited the expected P2X4-mediated inward current responses in oocytes expressing P2X4. A Ca^{2+}-free bath solution was used to prevent P2X4-mediated calcium entry and activation of endogenous calcium-activated chloride channels. Thus, under these experimental conditions we can assume that the inward currents observed upon ATP application at a holding potential of −60 mV result from Na^+ influx through activated P2X4 channels. In control oocytes, application of 100 µM ATP had no appreciable effect on whole-cell currents (Fig. 1 D; n = 25, N = 2). Repeated ATP applications resulted in a progressive decline of the P2X4 current response due to the known phenomenon of irreversible channel desensitization (Fountain and North, 2006). On average, the current responses to the second and third ATP application were reduced by 19 ± 2% and 39 ± 2%, respectively, compared with the current response elicited by the initial ATP application in the same recording (n = 14, N = 1; Fig. 1 A). Importantly, when t-DCA (250 µM) was present in the bath solution during the second ATP application (Fig. 1 B), the reduction in the second ATP response compared with the initial response was much more pronounced (82 ± 1%) than under control conditions in the absence of t-DCA. After t-DCA washout, the third ATP response recovered and was only 40 ± 2% smaller than the initial response. This reduction was similar to that of the third ATP response in the absence of t-DCA and can be attributed to irreversible channel desensitization (n = 20, N = 2; Fig. 1 B). Thus, these experiments demonstrate that t-DCA strongly and reversibly inhibits ATP-activated P2X4-mediated currents. Moreover, t-DCA does not seem to have any impact on the rate of P2X4 desensitization caused by repeated ATP applications. We also tested whether t-DCA applied alone for a prolonged period of time (60 s) affects P2X4 currents. As demonstrated in a representative recording in Fig. 1 C, t-DCA did not elicit any P2X4 currents, whereas subsequent application of ATP elicited a typical P2X4 current response. In summary, our results demonstrate that t-DCA has no effect on P2X4 per se but significantly inhibits ATP-activated P2X4-mediated currents.

Next we tested whether other common human bile acids—DCA, CA, CDCA, or the corresponding tauro-conjugated forms (t-CA, t-CDCA)—have similar effects on P2X4 currents as t-DCA. As discussed above, repeated ATP applications cause irreversible channel desensitization, which complicates the quantification of bile acid–mediated effects on the current response to ATP.

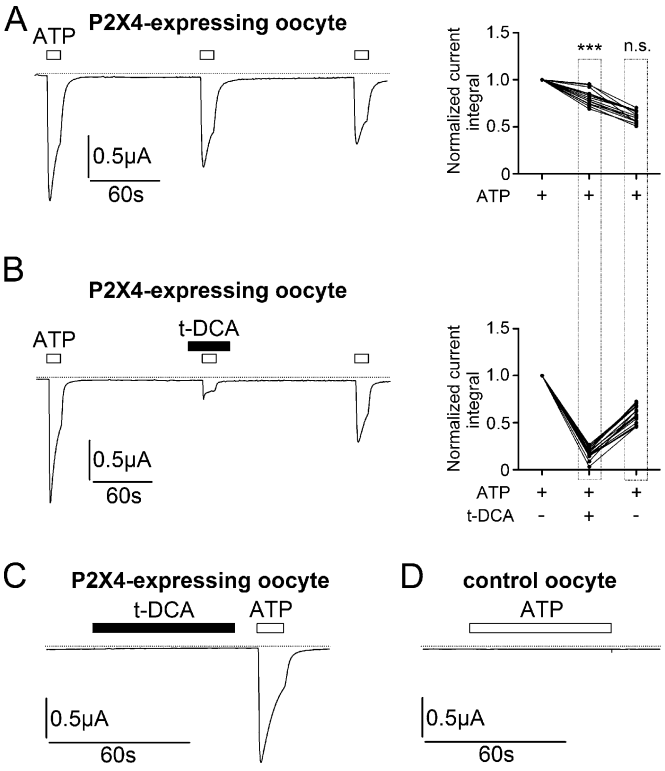

Figure 1. **Inhibition of ATP-activated P2X4-mediated currents by t-DCA. (A and B)** Left panels: Representative whole-cell current traces recorded in human P2X4-expressing oocytes. ATP (10 µM) and t-DCA (250 µM) were present in the bath solution as indicated by open and filled bars, respectively. Zero current level is indicated by a dotted horizontal line. Right panels: Summary of results from similar experiments as shown in the left panels (A: n = 14, N = 1; B: n = 20, N = 2). Lines connect data points obtained in the same experiment. To quantify current responses, the integral of the inward current elicited by ATP application below the baseline was determined for each response. The current integral values of the second and third ATP-activated responses were normalized to the current integral of the first response in each individual recording (normalized current integral). ***, Second normalized responses in A and B are significantly different ($P < 0.001$). n.s., not significant. Third normalized responses in A and B are not significantly different; Student's ratio t test. **(C)** Representative whole-cell current trace recorded in a human P2X4-expressing oocyte. ATP (10 µM) and t-DCA (250 µM) were present in the bath solution as indicated by open and filled bars, respectively. Zero current level is indicated by a dotted horizontal line (n = 25, N = 2). **(D)** Representative whole-cell current trace recorded in a control oocyte. ATP (100 µM) was present in the bath solution as indicated by open bar. Zero current level is indicated by a dotted horizontal line (n = 25, N = 2).

Therefore, we modified the experimental protocol for all subsequent experiments and applied ATP (10 µM) only once on each individual P2X4-expressing oocyte. In matched oocytes from the same batch ATP was applied in an alternating manner either in the presence or in the absence of bile acid (Fig. 2). ATP was typically applied ∼10 s after the beginning of the whole-cell current recording. As shown in Fig. 2 A, t-DCA (250 µM) significantly reduced the ATP-activated P2X4-mediated current response compared with that of control oocytes, on average by 68 ± 3% ($P < 0.001$, n = 20, N = 2). This finding further confirms the inhibitory effect of t-DCA on P2X4 observed using the experimental protocol with repeated ATP applications (Fig. 1 B).

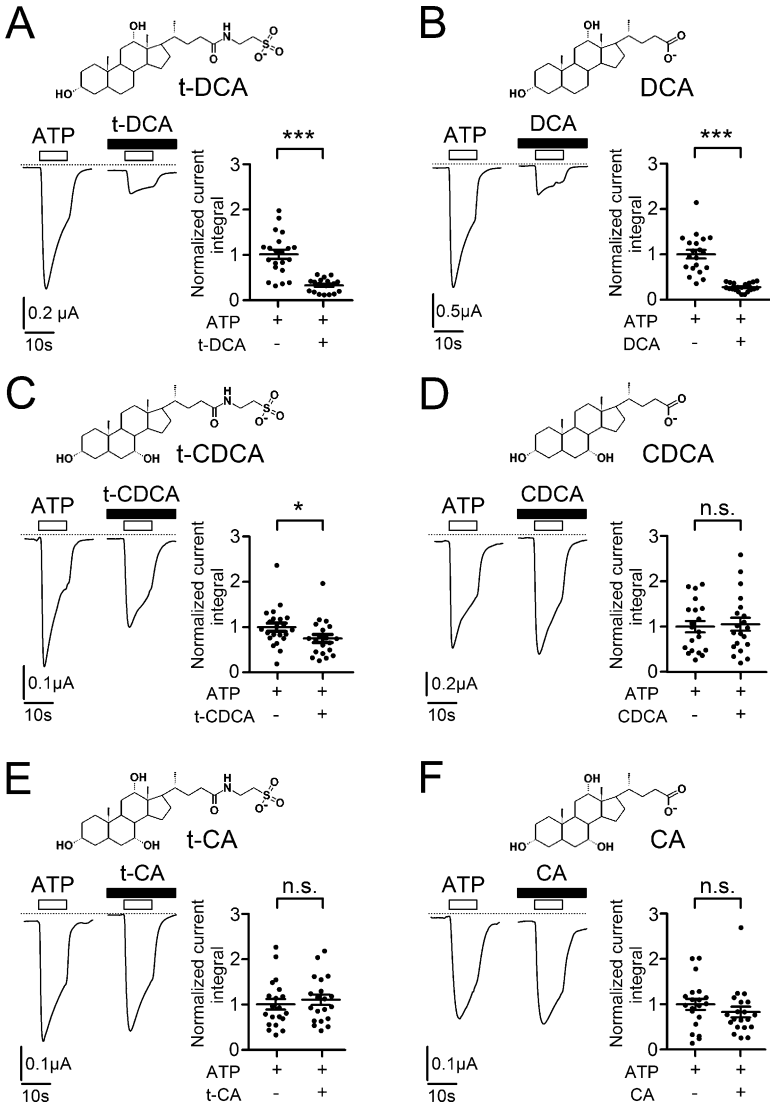

Figure 2. **DCA in tauro-conjugated or unconjugated form has the strongest inhibitory effect on P2X4 among the bile acids tested. (A–F)** Left panels: Representative whole-cell current traces recorded in human P2X4 expressing oocytes. ATP (10 µM) and bile acids (A: t-DCA; B: DCA; C: t-CDCA; D: CDCA; E: t-CA; F: CA; all in a concentration of 250 µM) were present in the bath solution as indicated by open and filled bars, respectively. Zero current level is indicated by a dotted horizontal line. Right panels: Summary of results from similar experiments as shown in the corresponding left panels. The ATP-activated current integral was calculated in each recording as described in Fig. 1 and normalized to the mean current integral determined in matched control oocytes (i.e., in the absence of bile acids) from the corresponding batch of oocytes (normalized current integral). Mean ± SEM values and individual data points are shown ($20 \le n \le 21$; $N = 2$); ***, *, Significantly different, $P < 0.001$ and $P < 0.05$, respectively; n.s., not significant; Student's ratio *t* test.

Co-application of ATP with unconjugated DCA (250 µM) had a similar 73 ± 2% inhibitory effect on P2X4 ($P < 0.001$, $n = 20$, $N = 2$; Fig. 2 B). This indicates that the taurine moiety of t-DCA does not play an important role in mediating the inhibitory effect of t-DCA on P2X4. The inhibitory effect of 250 µM t-CDCA was only 25 ± 9% ($P < 0.05$, $n = 21$, $N = 2$; Fig. 2 C). In the same concentration, CDCA (Fig. 2 D), t-CA (Fig. 2 E), or CA (Fig. 2 F) had no significant effect on P2X4-mediated currents. In additional experiments ($n = 20$, $N = 2$), we increased the concentration of CDCA, t-CA, and CA up to 500 µM. However, even in this high concentration, these bile acids did not significantly alter P2X4-mediated currents. In conclusion, among the bile acids tested, DCA and t-DCA had the most potent inhibitory effect on P2X4.

To estimate the apparent affinity of P2X4 to t-DCA, we tested the inhibitory effect of t-DCA using six different concentrations: 10 µM, 31 µM, 63 µM, 125 µM, 250 µM, and 500 µM. A t-DCA concentration higher than 500 µM was not used, because it may compromise the integrity of the plasma membrane of the oocytes. To avoid the channel rundown, we used matched oocytes from the same batch and applied ATP (10 µM) only once on each individual P2X4-expressing oocyte either in the absence or presence of different t-DCA concentrations. As evident from representative current traces shown in Fig. 3 A, P2X4-mediated currents were inhibited by t-DCA in a concentration-dependent manner. The summary of the data demonstrated that a saturating concentration of t-DCA was not reached (Fig. 3 B). With this limitation, we estimated a half maximal inhibitory concentration (IC_{50}) of ~160 µM.

Overall, our results demonstrate that DCA in unconjugated and tauro-conjugated form significantly reduces P2X4-mediated currents activated by ATP.

P2X4 affinity to ATP is not significantly changed in the presence of t-DCA

In further experiments, we characterized the inhibitory effect of t-DCA on P2X4 in more detail. To examine whether t-DCA affects the affinity of P2X4 to ATP, we investigated the concentration dependence of P2X4 activation by ATP under control conditions and in the presence of t-DCA (Fig. 4). To avoid channel rundown, we used matched oocytes from the same batch and applied ATP only once on each individual

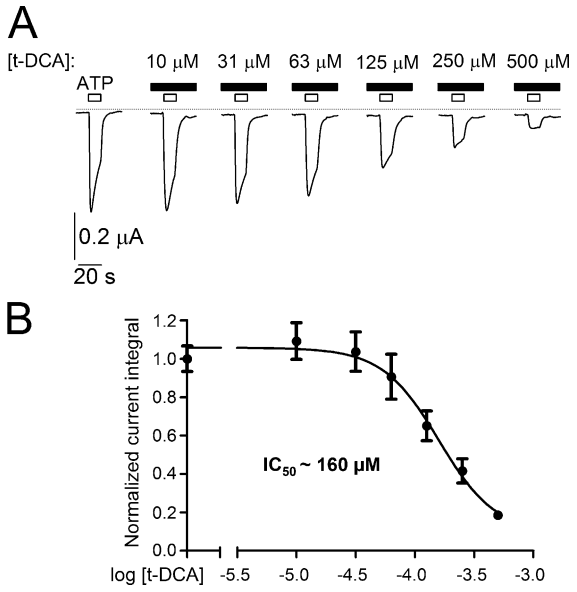

Figure 3. **Concentration-dependent inhibition of ATP-activated P2X4 currents by t-DCA. (A)** Representative P2X4-mediated whole-cell current traces recorded in individual matched oocytes from the same batch of oocytes in the absence of t-DCA or in the presence of t-DCA in the indicated concentrations. ATP (10 μM) and t-DCA were present in the bath solution as indicated by open and filled bars, respectively. Zero current level is indicated by a dotted horizontal line. **(B)** Concentration–response relationship of the inhibitory effect of t-DCA on ATP-activated P2X4 currents. Summary of normalized ATP-activated P2X4 current responses from similar experiments as shown in A. The current integral of each recording was normalized to the mean current integral obtained under control conditions (i.e., in the absence of t-DCA) for the corresponding batch of oocytes. Data are means ± SEM ($25 \le n \le 26$; $N = 3$) and were fitted to Eq. 1. IC_{50}, half maximal inhibitory concentration.

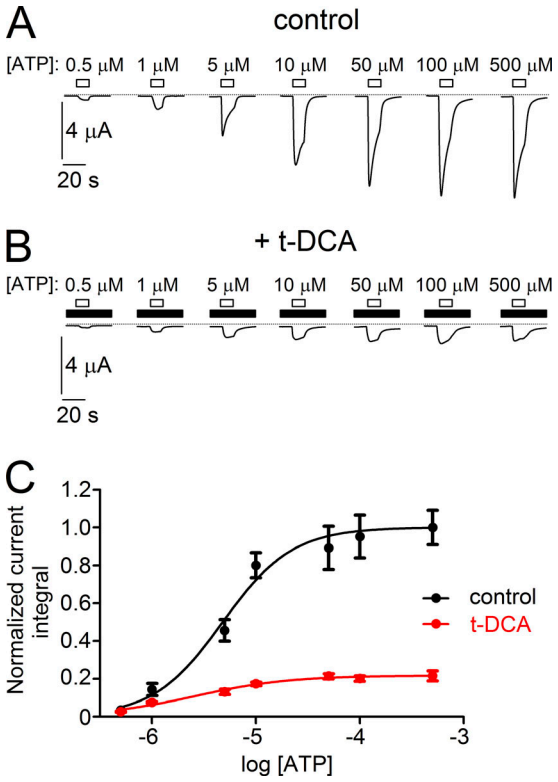

Figure 4. **Concentration-dependent stimulation of P2X4 by ATP under control conditions and in the presence of t-DCA in the bath solution. (A and B)** Representative P2X4-mediated whole-cell current traces recorded in matched oocytes from the same batch stimulated by ATP applied in the indicated concentrations in the absence (A) or presence (B) of t-DCA (250 μM) in the bath solution. ATP and t-DCA were present in the bath solution as indicated by open and filled bars, respectively. Zero current level is indicated by a dotted horizontal line. **(C)** Summary of results from similar experiments as shown in A and B and concentration–response curves of ATP-dependent stimulation of P2X4 currents recorded under control conditions (control, black symbols) or in the presence of t-DCA (t-DCA, red symbols). The current integral of each recording was normalized to the mean current integral obtained with 500 μM ATP applied under control conditions (i.e., in the absence of t-DCA) for the corresponding batch of oocytes (normalized current integral). Data are means ± SEM ($n = 12$, $N = 2$) and were fitted to Eq. 1.

P2X4-expressing oocyte either in the absence or presence of t-DCA (250 μM) using different ATP concentrations. Increasing the concentration of ATP from 0.5 to 500 μM resulted in the expected progressive increase in the mean magnitude of P2X4-mediated currents (Fig. 4, A and B). The estimated apparent affinity of ATP to P2X4 (half maximal effective concentration [EC_{50}] = 4.8 ± 1.2 μM; $n = 12$, $N = 2$; Fig. 4 C) was close to that observed in previous studies (Garcia-Guzman et al., 1997; Priel and Silberberg, 2004; Samways et al., 2011). Importantly, in the presence of t-DCA, the apparent affinity of ATP to P2X4 (EC_{50} = 2.4 ± 1.3 μM; $n = 12$, $N = 2$; Fig. 4 C) was similar to that under control conditions, whereas the efficacy of ATP to activate P2X4 currents was dramatically reduced. Thus, t-DCA–mediated inhibition of P2X4 is due to reduced efficacy but not affinity of ATP.

t-DCA stabilizes the closed state of P2X4

To investigate how t-DCA affects P2X4 channel function, we used the outside-out configuration of the patch-clamp technique. For better patch stability these recordings were performed in Ca^{2+}-containing ND96 solution. A possible activation of endogenous calcium–activated chloride channels by P2X4-mediated Ca^{2+} influx was prevented by the presence of EGTA in the pipette solution. In outside-out patches from control oocytes, application of ATP (100 μM) did not activate any endogenous currents (Fig. 5 A; $n = 16$, $N = 2$), consistent with our whole-cell current recordings from control oocytes (see Fig. 1 D). Fig. 5 B shows a representative recording from an outside-out patch excised from an oocyte expressing P2X4. In the absence of ATP no channel activity was detected. In contrast, exposure of the patch to ATP (100 μM) elicited a transient inward current response caused by the simultaneous activation of many P2X4 channels present in the patch. In ensemble current recordings like this, individual single-channel current events could not be resolved due to a high density of P2X4 channels present in the plasma membrane. In the continuous presence of ATP the peak response was followed by a spontaneous decline of channel activity due to the known phenomenon of channel inactivation (Coddou et al., 2011b). After ATP washout, a small residual channel activity persisted. Compared with the rapid onset of the ATP-induced current response in whole-cell recordings, the

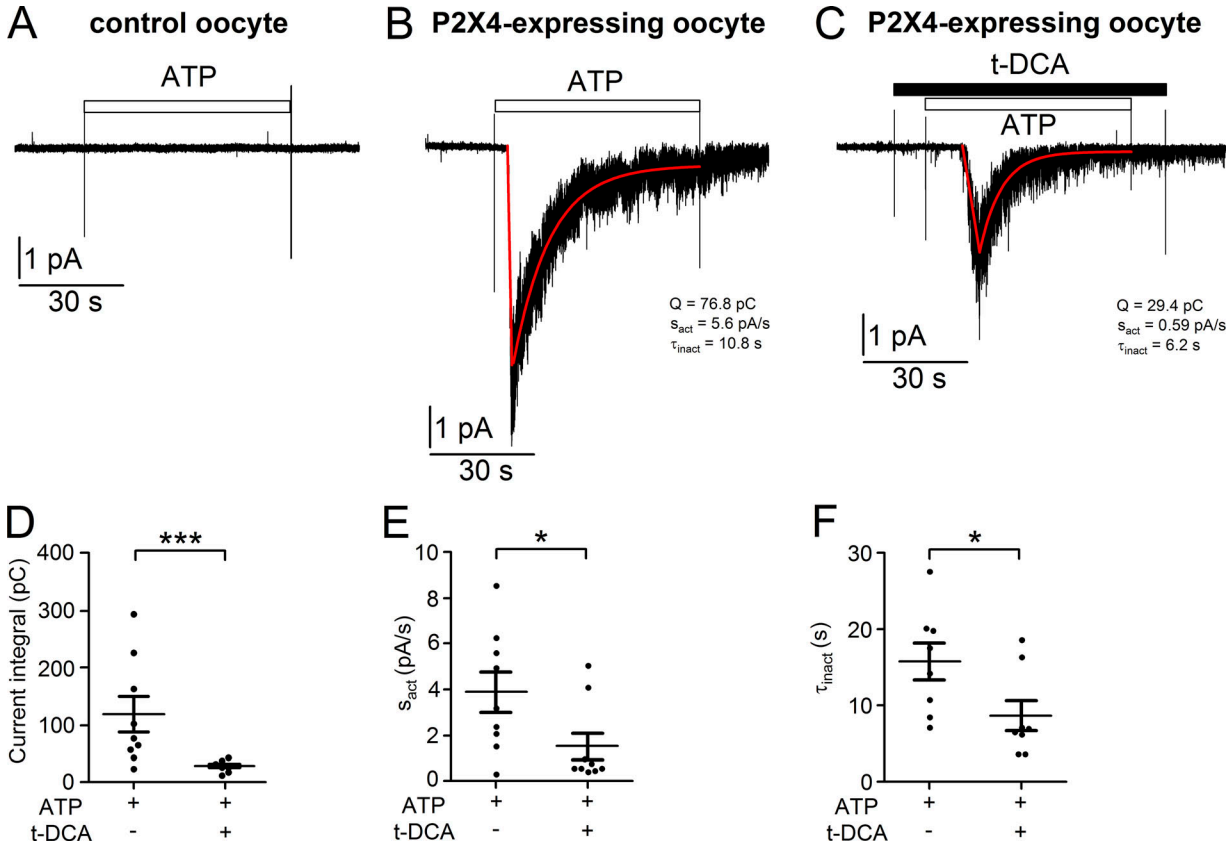

Figure 5. **t-DCA slows down the ATP-mediated activation of ensemble P2X4 currents and facilitates the spontaneous inactivation of the channel.** **(A)** Representative continuous current trace recorded at a holding potential of −70 mV from an outside-out patch obtained from a control oocyte. Application of ATP (100 µM) is indicated by an open bar. **(B and C)** Representative continuous current traces recorded at a holding potential of −70 mV from outside-out patches obtained from an oocyte expressing P2X4. Application of ATP (100 µM) and t-DCA (250 µM) is indicated by open and filled bars, respectively. Linear fit of initial phase of ATP-activated currents and exponential decay fit of the subsequent spontaneous current decrease were calculated as described in Materials and methods and delineated in red. To quantify the responses, the current integral (Q, pC), the slope of the initial P2X4-mediated ensemble inward current increase (s_{act}, pA/s), and the time constant of the spontaneous P2X4 ensemble current inactivation (τ_{inact}, s) were determined for each recording. **(D–F)** Summary of results from similar experiments as shown in B and C. Data are means ± SEM and individual data points (n = 9, N = 5). ***, *, Significantly different, P < 0.001 and P < 0.05, respectively (Student's t test).

peak response to ATP was somewhat delayed in outside-out patches. The delay time from switching to ATP containing bath solution to the onset of the peak response was, on average, ∼14 s, ranging 4–22 s. It is unlikely that this long and variable delay of the ATP response was caused by solution exchange artifacts, because the experimental setup ensured a reasonably rapid solution exchange at the patch after a constant delay time of ∼3 s due to the dead volume of the fluid exchange system (see Materials and methods). However, we have to consider the possibility that in excised patches the accessibility of ATP to P2X4 may be restricted or that patch excision alters the activation kinetics of P2X4 by unknown mechanisms. Interestingly, a second application of ATP to an outside-out patch usually resulted in the activation of only very few channels, even when the first ATP application elicited a sizable ensemble current response. Thus, irreversible channel desensitization after ATP exposure appeared to be more pronounced in outside-out patches than in whole-cell recordings. At present, we cannot provide an explanation for these differences, but our observations are consistent with the previously reported finding that P2X4 function is slightly altered and less stable in excised patches compared with intact cells (Priel and Silberberg, 2004). Nevertheless, the ATP-activated P2X4-mediated ensemble current response in outside-out patches was overall similar to that observed in whole-cell current recordings (see Fig. 2 A).

To validate our finding from whole-cell recordings, we tested whether t-DCA also inhibits P2X4-mediated ensemble currents in outside-out patches. To avoid the problem of irreversible P2X4 inactivation after ATP exposure, individual patches were exposed only once to ATP either in the presence or absence of t-DCA (250 µM). As shown in the representative current trace in Fig. 5 C, t-DCA significantly reduced the ATP-activated P2X4-mediated current response (29.4 pC) compared with the control response (76.8 pC) in the absence of t-DCA (Fig. 5 B). On average, t-DCA caused a significant 76 ± 3% reduction in the ATP-induced P2X4-mediated inward current response (P < 0.001, n = 9, N = 5; Fig. 5 D), which is in good agreement with the degree of inhibition observed in the whole-cell current recordings. The initial linear phase of the peak response elicited by ATP was fitted with a linear function (Eq. 2; see Materials and methods) to estimate

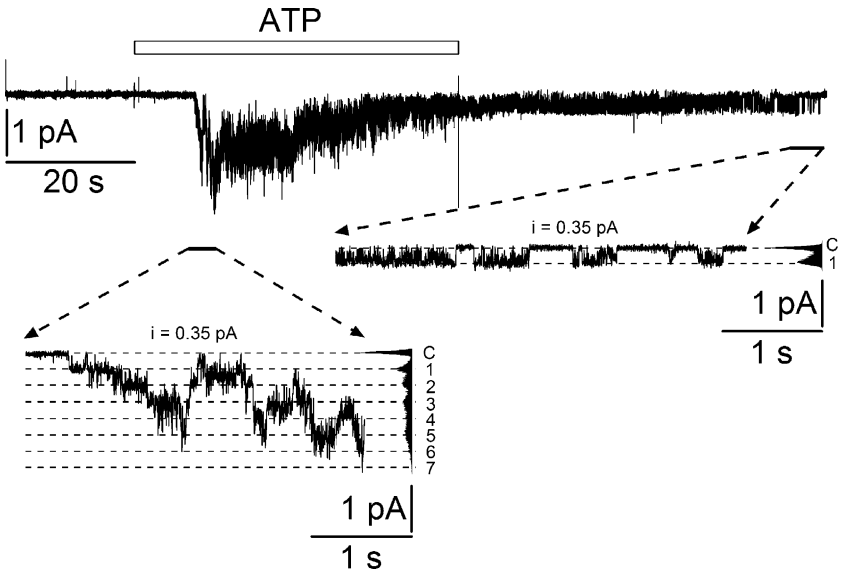

Figure 6. **ATP-activated P2X4-mediated current response with single-channel events recorded from an outside-out patch.** Representative continuous current trace recorded at a holding potential of −70 mV from an outside-out patch of a P2X4-expressing oocyte. Application of ATP (100 µM) is indicated by an open bar. The insets show the indicated fragments of the current trace on an expanded time scale. Binned current amplitude histograms are shown on the right side of the insets and were obtained from the corresponding parts of the trace to calculate single-channel current amplitude (i). The current level at which all channels are closed (C) was determined at the beginning of the trace before ATP application. Dotted lines in the insets indicate channel open levels (1–7).

the slope of the initial P2X4-mediated inward current increase (s_{act}, pA/s). The subsequent current decline was fitted with an exponential decay function (Eq. 3; see Materials and methods) to estimate the time constant of P2X4 current inactivation (τ_{inact}, s). As illustrated by the representative traces in Fig. 5, B and C, the slope of the ATP-activated current increase was considerably reduced in the presence of t-DCA (0.59 pA/s) compared with control conditions (5.6 pA/s). Moreover, the spontaneous current inactivation was faster in the presence of t-DCA than in its absence, with time constants of 6.2 s and 10.8 s, respectively (Fig. 5, B and C). Summarizing results from similar experiments confirmed that the slope of the initial P2X4-mediated inward current increase (Fig. 5 E) and the time constant of the subsequent current decline (Fig. 5 F) were significantly decreased in the presence of t-DCA compared with control. These results indicate that t-DCA slows down ATP-induced P2X4 channel activation and facilitates subsequent channel inactivation.

The altered kinetics of the ensemble current response to ATP in the presence of t-DCA suggest that t-DCA stabilizes the closed state of P2X4. To confirm this, we studied P2X4 single-channel activity in outside-out patches. To increase the likelihood of resolving single-channel events, we reduced the expression level of P2X4 by reducing the amount of cRNA injected per oocyte from 5 to 2 ng. This reduced channel density at the plasma membrane and hence the number of active channels per patch. Fig. 6 shows a recording from an outside-out patch with a current response to ATP during which single-channel events could be resolved as illustrated in the insets. In the initial phase of the response, up to seven apparent channel levels were detected (left inset of Fig. 6). After ATP washout at the end of the recording, only one channel remained active in the patch with occasional bursts of channel openings (right inset of Fig. 6). The amplitude histogram revealed a single-channel current amplitude of ∼0.35 pA. At a trans-patch potential of −82 mV this corresponds to a single-channel conductance of ∼4.3 pS. This is lower than the conductance of ∼9 pS reported for human P2X4 in Mg^{2+}-free bath solution containing 140–150 mM Na^+ (Evans, 1996; Negulyaev and Markwardt, 2000). This latter Na^+ concentration is ∼50% higher than the Na^+ concentration of 96 mM used in the present study. Moreover, our bath solution contained 1 mM Mg^{2+}, which significantly reduces the conductance of P2X4 (Negulyaev and Markwardt, 2000). These experimental differences may well explain the lower single-channel conductance in our recordings. Taken together, our findings support the conclusion that the current response elicited by ATP is due to the activation of P2X4 channels.

The reduced P2X4 expression level allowed us to obtain several recordings with only one apparent active single channel in the patch (Fig. 7). These patches were used to analyze the effects of t-DCA on single-channel properties of P2X4 including single-channel kinetics. To activate P2X4, ATP was applied for 60 s in the absence (Fig. 7 A) or presence (Fig. 7 B) of t-DCA. As mentioned above, the onset and duration of the ATP response varied from patch to patch. Therefore, we focused our analysis on the middle portion (∼20 s) of the current traces recorded during a 60-s exposure to ATP. In this middle portion, single-channel activity was observed in all patches analyzed. The estimated single-channel current amplitude of channels in patches with only one apparent active channel was similar to that observed in patches with several active P2X4 channels, which confirms the molecular identity of these channels. Single-channel current amplitude was not significantly affected by t-DCA (Fig. 7 C). In contrast, P_o was significantly decreased by t-DCA (Fig. 7 D). To reveal an effect of t-DCA on single-channel kinetics, dwell times were analyzed using a half-amplitude threshold crossing algorithm to detect individual channel closing and opening events (see Materials and methods). For each group of patches (i.e., patches with or without t-DCA application), dwell-time data from individual patches (n = 7/group; N = 5) were combined and subsequently analyzed together. These combined dwell-time data confirmed that P_o was about threefold higher under control conditions (∼0.28) than in the presence of t-DCA (∼0.09). This is consistent with the P_o data shown in Fig. 7 D, which were estimated

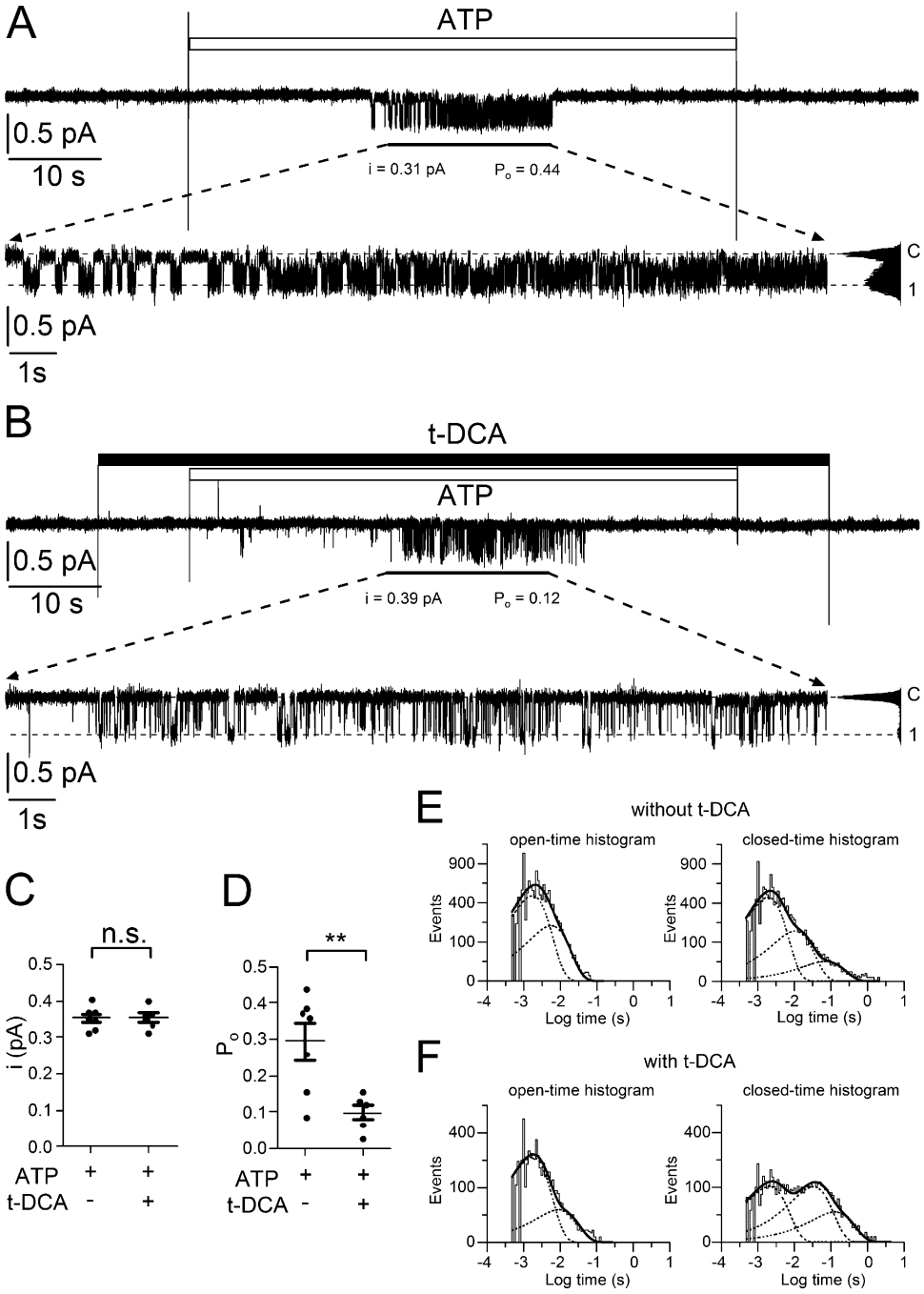

Figure 7. **t-DCA stabilizes the closed state of P2X4. (A and B)** Examples of continuous current traces recorded at a holding potential of −70 mV from outside-out patches in which ATP activated only one P2X4 channel. Application of ATP (100 µM) and t-DCA (250 µM) is indicated by open and filled bars, respectively. The insets show the middle portions (~20 s) of the current traces during ATP exposure on an expanded time scale as indicated. Binned current amplitude histograms obtained from these portions are shown on the right side of the corresponding insets. They were used to determine the closed level of the channel (C) and the channel open level (1) indicated by the dotted lines and to calculate single-channel current amplitude (i). Channel open probability (P_o) was estimated from the time integral of inward current exceeding the channel closed level divided by the product of i and total duration of the analyzed portion. **(C and D)** Summary of results from similar experiments as shown in A and B. Data are means ± SEM and individual data points (n = 7/group, N = 5). **, Significantly different, P < 0.01; n.s., not significant; Student's t test. **(E and F)** Dwell-time histograms generated from combined dwell-time data obtained from current portions as marked in (A) and (B) using all experiments summarized in (C) and (D).

from individual patches using an alternative approach (see Materials and methods). Importantly, the dwell-time data revealed that the mean open time of the channel was not affected by t-DCA (3.6 ms under both conditions), whereas the mean closed time was about threefold higher in the presence of t-DCA (35 ms) than in its absence (9.4 ms). This indicates that t-DCA decreases channel P_o mainly by increasing the closed time of the channel.

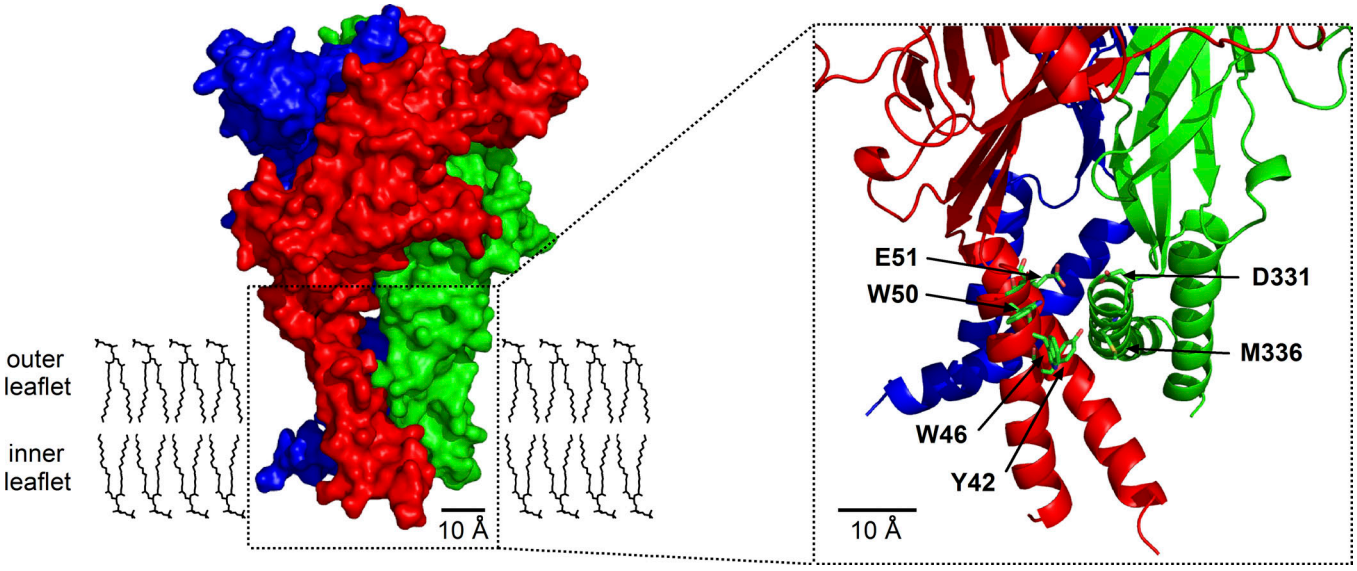

Figure 8. **Homology model of the transmembrane domains of human P2X4.** A homology model of human P2X4 was generated based on the crystal structure of *D. rerio* P2X4.1 in the closed state. A molecular surface representation of human P2X4 (side view) is shown in the left panel. To visualize the individual subunits of the P2X4 homotrimer, they are colored in red, green, and blue. The putative location of the plasma lipid bilayer (outer and inner leaflet) is schematically depicted with DPPC molecules in sticks representation. The inset shows the channel transmembrane domains on an expanded scale in cartoon representation using the same color code for the individual subunits. Amino acid residues that were substituted by alanine and tested experimentally are indicated with arrows and shown in stick representation with carbons in green, sulfur in yellow, nitrogens in blue, and oxygens in red. DPPC, dipalmitoylphosphatidylcholine.

To investigate this further, dwell-time histograms were generated from recordings in the absence (Fig. 7 E) and presence (Fig. 7 F) of t-DCA using a logarithmic time axis and a square-root scaling for the number of events on the ordinate as described by Sigworth and Sine (1987). Two open-time constants and three closed-time constants were estimated from these histograms. The estimated open-time constants and their percentage contributions were 1.7 ms (76%) and 5.6 ms (24%) in the absence of t-DCA and 1.7 ms (87%) and 9.2 ms (13%) in the presence of t-DCA. Thus, t-DCA had little effect on open-time constants and their relative distribution. In contrast, t-DCA markedly altered the closed-time histogram. The estimated closed-time constants and their percentage contributions were 1.9 ms (71%), 10.4 ms (25%), and 70.7 ms (4%) in the absence of t-DCA and 2.0 ms (44%), 32.5 ms (43%), and 125.3 ms (13%) in the presence of t-DCA. Thus, t-DCA did not result in the appearance of an additional closed-time constant but extended the two longer closed-time constants by a factor of about two to three. Importantly, t-DCA decreased the percentage contribution of the short closed-time constant and substantially increased the percentage contributions of the two longer closed-time constants. Taken together, these findings indicate that t-DCA inhibits P2X4 by favoring the closed state of the channel.

Tryptophan (W46), aspartate (D331), and methionine (M336) located in the transmembrane domains are critically involved in t-DCA–mediated inhibition of P2X4

In an attempt to identify amino acid residues that are functionally relevant for the t-DCA effect on P2X4 we used a site-directed mutagenesis approach and replaced several candidate residues in the two transmembrane domains (TM1 and TM2) of the channel by alanine. The individually mutated residues are indicated in the homology model of human P2X4 (Fig. 8), which we generated based on the crystal structure of *D. rerio* P2X4 in its closed state (Hattori and Gouaux, 2012). The residues E51 in TM1 and D331 in TM2 were selected because they are located in a region of P2X4 that resembles a region of ENaC/DEG channels that we previously identified as a potential bile acid interaction site (Ilyaskin et al., 2016, 2017, 2018). In addition, we mutated several residues that have been reported to be functionally important for P2X4 modulation by IVM and are located in TM1 (Y42, W46, W50) or TM2 (D331, M336) of P2X4 (Asatryan et al., 2010; Popova et al., 2013). With the exception of the Y42A mutant, which for unknown reasons could not be functionally expressed, we detected typical ATP-induced P2X4 current responses in all other mutant channels. The current responses of the mutant channels to ATP were qualitatively similar to the response observed in WT P2X4 (Fig. 9, A–F). As summarized in Fig. 9 G, the size of the ATP-induced P2X4 current response was reduced by all tested mutations except for D331A. This may have various reasons, e.g., reduced expression, impaired trafficking, or decreased ATP affinity of the mutant channels, but was not further investigated. The relative inhibitory effect of t-DCA on the ATP-induced P2X4 current response was fully preserved in the E51A (Fig. 9 B) and W50A (Fig. 9 D) mutant channels and averaged 74% and 63%, respectively (Fig. 9 H), which was similar to the 70% inhibition observed in matched control experiments with WT P2X4 (Fig. 9 A). In contrast, the relative inhibitory effect was significantly reduced by the D331A (Fig. 9 C) and the M336A (Fig. 9 E) mutations, averaging only 38% and 22%, respectively (Fig. 9 H). Importantly, the W46A mutation not only abolished the inhibitory effect of t-DCA on the ATP-induced

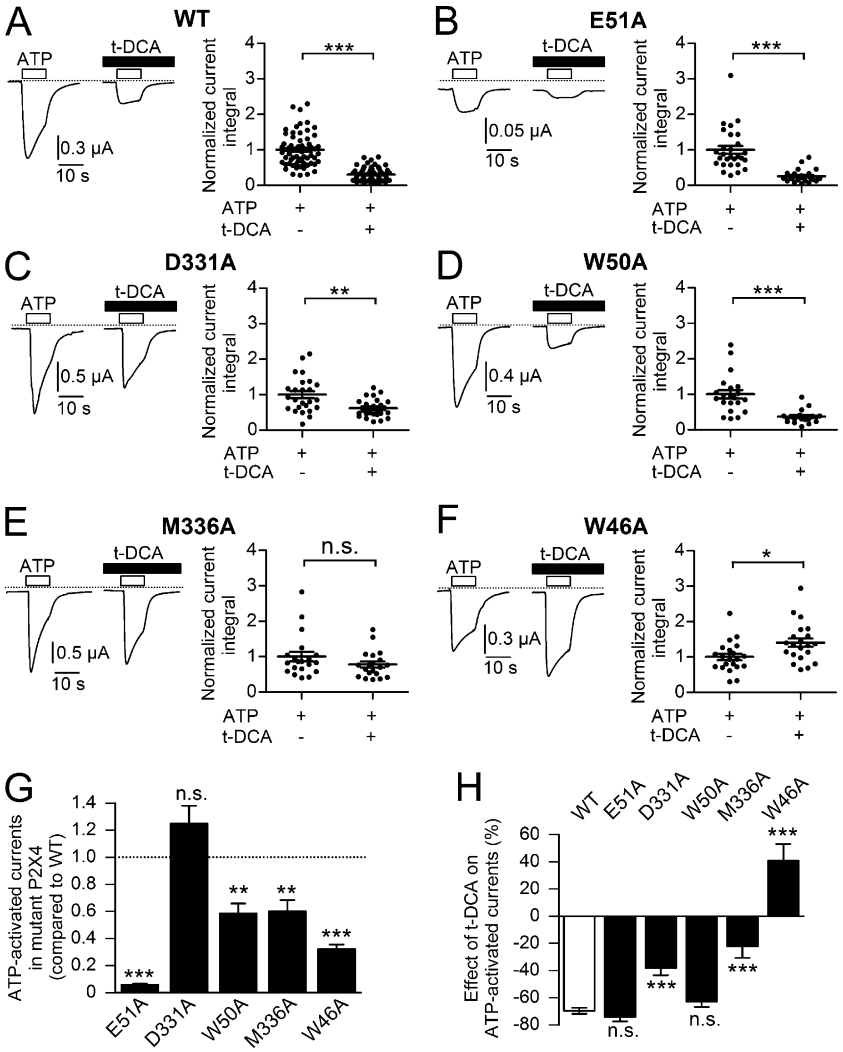

Figure 9. **D331, M336, and W46 are critically involved in t-DCA–mediated inhibition of P2X4. (A–F)** Left panels: Representative whole-cell current traces recorded in oocytes expressing human WT (A) or mutant (B: E51A; C: D331A; D: W50A; E: M336A; F: W46A) P2X4. ATP (10 μM) and t-DCA (250 μM) were present in the bath solution as indicated by open and filled bars, respectively. Zero current level is indicated by a dotted horizontal line. Right panels: Summary of results from similar experiments as shown in the corresponding left panels. Current integrals were normalized as described in Fig. 2. Values are means ± SEM and individual data points are shown (A: n = 65; N = 7; B: n = 28; N = 3; C: n = 25; N = 3; D: n = 21; N = 2; E: n = 20; N = 2; F: n = 21; N = 2); ***, **, *, Significantly different, P < 0.001, P < 0.01, and P < 0.05, respectively; n.s., not significant; Student's ratio t test. **(G)** Basal ATP-activated currents of mutant P2X4 channels compared with WT P2X4 from the same experiments as shown in A–F. The ATP-activated current integral was calculated in each recording and was normalized to the mean current integral determined in matched control oocytes (i.e., expressing WT P2X4) from the corresponding batch of oocytes (normalized to WT). Data are means ± SEM. ***, **, Significantly different compared with WT, P < 0.001 and P < 0.01, respectively; n.s., not significant; one-way ANOVA with Bonferroni post hoc test. **(H)** Relative effects of t-DCA on ATP-activated P2X4 currents (negative values indicate inhibition; positive values indicate stimulation) in oocytes expressing WT P2X4 or different P2X4 mutant channels. The current integral calculated in each recording was normalized as described in Fig. 2. Data are means ± SEM of the normalized current integrals in the presence of t-DCA from the same experiments as shown in A–F. ***, Significantly different compared with WT, P < 0.001; n.s., not significant; one-way ANOVA with Bonferroni post hoc test.

P2X4 current response but converted it to a stimulatory effect (Fig. 9 F). Indeed, in experiments with the W46A mutant channel, the ATP-induced P2X4 current response was, on average, 41% higher in the presence of t-DCA than in its absence (Fig. 9 H). Overall, these data suggest that t-DCA functionally interacts with several amino acid residues within the transmembrane domains of P2X4, thereby stabilizing the closed conformation of the channel.

Docking simulations suggest that binding of t-DCA to the transmembrane domains of P2X4 involves the residues W46, D331, and M336

Our mutagenesis experiments demonstrated that the residues W46, D331, and M336 contribute to mediating the inhibitory effect of t-DCA on P2X4 currents. To obtain a molecular model for a possible interaction of t-DCA with the transmembrane region of the channel in which these residues are localized, we used a molecular docking approach. The homology model of human P2X4 in the closed state predicts that these residues form a cleft between adjacent subunits with W46 positioned in TM1 of one subunit and D331 and M336 in TM2 of the other subunit (Fig. 10 A). Molecular-docking simulations were performed and predicted that t-DCA molecules may occupy this cleft (Fig. 10 B). An overlay of the generated docking modes revealed a prominent cluster of t-DCA molecules bound to residues W46, D331, and M336. This is consistent with the hypothesis that t-DCA may directly interact with this channel region. Structural information suggests that, in its open conformation, the transmembrane domains of P2X4 are moved further apart (Hattori and Gouaux, 2012). This probably results in the elimination of the putative bile aci d binding site as suggested by the model shown in Fig. 10 C. This model predicts that the binding of t-DCA to the putative bile acid binding site within the channel transmembrane domains is only feasible in the closed state of the channel.

Discussion

In this study, we demonstrated that unconjugated DCA and its tauro-conjugated form (t-DCA) strongly inhibit ATP-activated P2X4-mediated currents in *X. laevis* oocytes. Thus, DCA/t-DCA are potent negative modulators of P2X4 function. Moreover, using outside-out patch-clamp measurements and site-directed mutagenesis, we revealed a possible molecular mechanism of t-DCA–mediated inhibition of P2X4 activity.

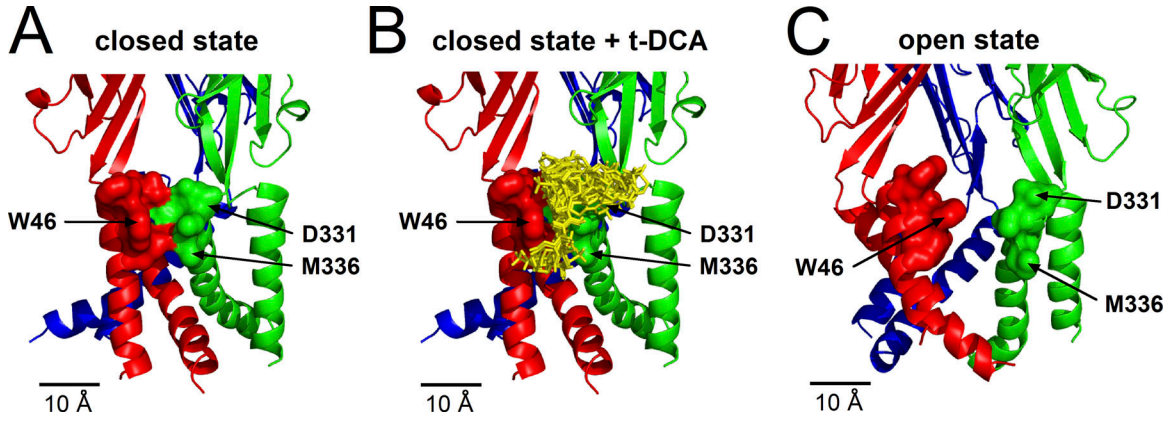

Figure 10. **Docking simulation predicts a putative t-DCA binding site in the intersubunit interface of P2X4 transmembrane domains in the closed state of the channel. (A and B)** For docking simulations, the same homology model of human P2X4 in the closed state was used as shown in Fig. 8. Amino acid residues forming the putative bile acid binding site are shown in molecular surface representation without (A) and with (B) docked t-DCA molecules. An overlay of 30 out of 100 similar t-DCA docked modes is depicted in yellow stick representation. Our functional studies suggested that the amino acid residues indicated with arrows are involved in mediating the inhibitory effect of t-DCA on P2X4. **(C)** Homology model of human P2X4 in the open state showing the same channel region as in A and B.

We have previously investigated the effects of bile acids on several ion channels belonging to the ENaC/DEG ion channel family (Ilyaskin et al., 2016, 2017, 2018). Notably, t-DCA strongly stimulated the activity of human ENaC in the αβγ and δβγ subunit configuration (Ilyaskin et al., 2016) and of human BASIC (Ilyaskin et al., 2018). Moreover, t-DCA potentiated proton-activated ASIC1a currents (Ilyaskin et al., 2017). In view of the structural similarity between P2X4 and ASIC1 (Gonzales et al., 2009), we hypothesized that t-DCA may also affect ATP-activated P2X4 currents. Interestingly, and in contrast to its stimulatory effect on currents mediated by members of the ENaC/DEG family of ion channels, t-DCA strongly inhibited P2X4 currents. This indicates that t-DCA can also modulate the function of P2X4 but with an inhibitory rather than stimulatory effect.

Outside-out patch-clamp recordings revealed the effects of t-DCA on P2X4 function at the single-channel level. We demonstrated that in the presence of t-DCA, P2X4 single-channel activity (i.e., its open probability, P_o) was significantly reduced compared with control conditions. Theoretically, the decreased P_o of P2X4 by t-DCA may be explained by a decreased duration of channel openings (destabilization of the channel open state) and/or an increased channel dwelling time in the closed state (stabilization of the channel closed state). Analysis of single-channel kinetics using dwell-time histograms demonstrated that t-DCA has little effect on the open-time constants and their relative distribution. In contrast, t-DCA had a marked effect on the closed-time histogram and, in particular, increased the percentage contributions of the longer closed-time constants. Therefore, we conclude that t-DCA stabilizes the closed state of P2X4. In contrast, we have shown that t-DCA stabilizes the open state of BASIC, which explains the observed stimulatory effect of t-DCA on BASIC (Ilyaskin et al., 2018). In addition, t-DCA significantly changed the single-channel current amplitude of ENaC/DEG ion channels, indicating that t-DCA may interact with a region close to the channel pore (Ilyaskin et al., 2016, 2017, 2018). In concordance with this hypothesis, we demonstrated that the substitution of a single amino acid residue within the second transmembrane domain of the ENaC/DEG ion channels (in the so-called degenerin region) significantly reduced the stimulatory effect of t-DCA (Ilyaskin et al., 2016, 2017, 2018). In the present study, t-DCA did not significantly change the single-channel current amplitude of P2X4, which suggests that t-DCA does not affect the ion permeation pathway through the channel. Moreover, the results of site-directed mutagenesis indicate that t-DCA may bind to P2X4 at a protein–membrane interface of the channel's transmembrane domains rather than in the direct vicinity of the channel pore. Importantly, we demonstrated that the amino acid residues W46, D331, and M336 are critically involved in mediating the functional effect of t-DCA on P2X4. These residues are localized in TM1 and TM2, respectively, and are positioned at the level of the outer leaflet of the plasma membrane. Our docking simulations support the concept that these three residues contribute to a putative bile acid binding site localized in the transmembrane domains of P2X4. As discussed by Hattori and Gouaux (2012), the closed conformation of P2X4 is stabilized by several interactions between TM2 helices that include contacts between L340, L346, and A347. These residues are localized in close proximity to the putative bile acid binding site identified in the present study. It is tempting to speculate that binding of t-DCA to this binding site may strengthen the interaction of adjacent subunits, thereby further stabilizing the channel's closed state.

Bile acids are membrane-active substances (Helenius and Simons, 1975) and therefore their incorporation into the plasma membrane may potentially influence P2X4 function by modulating the physical properties of the membrane. Recently, it has been reported that another purinergic receptor rP2X2 can be modulated by diverse amphiphilic substances (Schmidt et al., 2018). The authors proposed that the observed effects were mainly due to membrane alterations in the presence of tested surface-active substances. However, a clear correlation between

the amphiphilic substance-mediated changes in membrane properties and alterations of P2X2 function was not observed (Schmidt et al., 2018). Thus, the observed effects may also be caused by specific interactions of membrane-active substances with the channel. To summarize, we cannot exclude the possibility that t-DCA inhibits P2X4 at least in part indirectly via a modulation of membrane characteristics. However, our site-directed mutagenesis experiments support the conclusion that the inhibitory effect of t-DCA involves a direct interaction with P2X4.

Interestingly, the putative t-DCA binding site in P2X4 is localized in the same channel region as the proposed interaction site for the positive P2X4 modulator IVM, a macrocyclic lactone (Habermacher et al., 2016). The mechanism of P2X4 potentiation by IVM is highly complex and not yet fully understood. Using site-directed mutagenesis, >20 amino acid residues (including Y42, W46, W50, E51, D331, and M336 tested in the current study) within the transmembrane domains of P2X4 have been shown to be involved in IVM sensitivity (Silberberg et al., 2007; Jelínkova et al., 2008; Asatryan et al., 2010; Samways et al., 2012; Popova et al., 2013). Computer molecular dynamics simulations predicted a direct binding of IVM at the intersubunit interface between Y42, W46, and W50 in TM1 and M336 in TM2 in the open state of P2X4 (Popova et al., 2013). Moreover, it has been experimentally confirmed that IVM stabilizes the open state of P2X4 (Priel and Silberberg, 2004). Our results suggest that W50 and E51 are not involved in t-DCA sensitivity of P2X4. This indicates that the IVM and t-DCA binding sites in P2X4 may partially overlap but are not identical. Taken together, these findings suggest that t-DCA interacts with D331, W46, and M336 in the closed state of P2X4, whereas IVM binds to the same amino acid residues but in the open state of the channel. Interestingly, the substitution of W46 by a nonaromatic amino acid like alanine switched the potentiating effect of IVM to inhibition (Popova et al., 2013). In the present study, we observed the opposite phenomenon: the W46A mutation converted the inhibitory effect of t-DCA on ATP-activated P2X4 currents into a stimulatory effect. Computer simulations of rP2X4 predicted π-π interactions between the aromatic rings of W46, Y42, and W50 (Popova et al., 2013). Thus, the disruption of these stack interactions by W46A substitution may disturb IVM-mediated potentiation as well as t-DCA–mediated inhibition of P2X4. However, at present, this remains a speculation. A structure of P2X4 co-crystallized with IVM and t-DCA may help to elucidate this further.

P2X4 is abundantly expressed in hepatocytes and cholangiocytes where its physiological role and regulation remain to be determined (Doctor et al., 2005; Besnard et al., 2016). In view of our findings, it is conceivable that in the liver and in bile ducts bile acids may play a role as local modulators of P2X4 function. Moreover, our findings indicate that the same channel region is involved in mediating the stimulatory effect of IVM and the inhibitory effect of t-DCA/DCA. Therefore, it is tempting to speculate that this channel region contains overlapping regulatory sites that may mediate P2X4 stimulation or inhibition depending on the molecular structure of the interacting substance. It will be a challenge of future research to identify naturally occurring amphiphilic/lipophilic substances or novel pharmacological compounds that can modify P2X4 function by interacting with this channel region. Such substances may act as physiologically relevant or therapeutically useful local P2X4 modulators, possibly in a tissue-specific manner.

In conclusion, our results demonstrate that t-DCA strongly inhibits P2X4 currents by stabilizing the closed state of the channel. This effect involves an interaction of the bile acid with a critical channel region in the intersubunit protein–membrane interface. The potential (patho-)physiological role of this novel mechanism of P2X4 regulation remains to be elucidated.

Acknowledgments

The expert technical assistance of Ralf Rinke is gratefully acknowledged. The authors also thank Prof. Heinrich Sticht and Prof. Tilmann Volk for their helpful advice regarding the homology modeling and analysis of single-channel kinetics, respectively.

This study was supported by the ELAN program of the FAU Interdisciplinary Center for Clinical Research (IZKF; grant 17-08-01-1-Ilyaskin/P015 to A.V. Ilyaskin) and by a grant of the Deutsche Forschungsgemeinschaft (HA 6655/1-1 to S. Haerteis).

The authors declare no competing financial interests.

Author contributions: A.V. Ilyaskin and F. Sure performed the experiments, analyzed the data, and prepared the figures. V. Nesterov contributed to the single-channel analysis. A.V. Ilyaskin, S. Haerteis, and C. Korbmacher designed and coordinated the study. The manuscript was written mainly by A.V. Ilyaskin and C. Korbmacher, but all authors contributed and approved the final version of the manuscript.

Kenton J. Swartz served as editor.

Submitted: 16 November 2018
Revised: 8 March 2019
Accepted: 22 March 2019

References

Asatryan, L., M. Popova, D. Perkins, J.R. Trudell, R.L. Alkana, and D.L. Davies. 2010. Ivermectin antagonizes ethanol inhibition in purinergic P2X4 receptors. *J. Pharmacol. Exp. Ther.* 334:720–728. https://doi.org/10.1124/jpet.110.167908

Bahima, L., J. Aleu, M. Elias, M. Martín-Satué, A. Muhaisen, J. Blasi, J. Marsal, and C. Solsona. 2006. Endogenous hemichannels play a role in the release of ATP from *Xenopus* oocytes. *J. Cell. Physiol.* 206:95–102. https://doi.org/10.1002/jcp.20440

Besnard, A., J. Gautherot, B. Julien, A. Tebbi, I. Garcin, I. Doignon, N. Péan, E. Gonzales, D. Cassio, B. Grosse, et al. 2016. The P2X4 purinergic receptor impacts liver regeneration after partial hepatectomy in mice through the regulation of biliary homeostasis. *Hepatology.* 64:941–953. https://doi.org/10.1002/hep.28675

Coddou, C., S.S. Stojilkovic, and J.P. Huidobro-Toro. 2011a. Allosteric modulation of ATP-gated P2X receptor channels. *Rev. Neurosci.* 22:335–354. https://doi.org/10.1515/rns.2011.014

Coddou, C., Z. Yan, T. Obsil, J.P. Huidobro-Toro, and S.S. Stojilkovic. 2011b. Activation and regulation of purinergic P2X receptor channels. *Pharmacol. Rev.* 63:641–683. https://doi.org/10.1124/pr.110.003129

Corriden, R., and P.A. Insel. 2010. Basal release of ATP: an autocrine-paracrine mechanism for cell regulation. *Sci. Signal.* 3:re1. https://doi.org/10.1126/scisignal.3104re1

Diakov, A., and C. Korbmacher. 2004. A novel pathway of ENaC activation involves an SGK1 consensus motif in the C-terminus of the channel's alpha-subunit. *J. Biol. Chem.* 279:38134–38142. https://doi.org/10.1074/jbc.M403260200

Diakov, A., V. Nesterov, M. Mokrushina, R. Rauh, and C. Korbmacher. 2010. Protein kinase B alpha (PKBα) stimulates the epithelial sodium channel (ENaC) heterologously expressed in *Xenopus laevis* oocytes by two distinct mechanisms. *Cell. Physiol. Biochem.* 26:913–924. https://doi.org/10.1159/000324000

Doctor, R.B., T. Matzakos, R. McWilliams, S. Johnson, A.P. Feranchak, and J.G. Fitz. 2005. Purinergic regulation of cholangiocyte secretion: Identification of a novel role for P2X receptors. *Am. J. Physiol. Gastrointest. Liver Physiol.* 288:G779–G786. https://doi.org/10.1152/ajpgi.00325.2004

Ebihara, L. 1996. *Xenopus* connexin 38 forms hemi-gap-junctional channels in the nonjunctional plasma membrane of *Xenopus* oocytes. *Biophys. J.* 71:742–748. https://doi.org/10.1016/S0006-3495(96)79273-1

Evans, R.J. 1996. Single channel properties of ATP-gated cation channels (P2X receptors) heterologously expressed in Chinese hamster ovary cells. *Neurosci. Lett.* 212:212–214. https://doi.org/10.1016/0304-3940(96)12804-4

Fausther, M., E. Gonzales, and J.A. Dranoff. 2012. Role of purinergic P2X receptors in the control of liver homeostasis. *Wiley Interdiscip. Rev. Membr. Transp. Signal.* 1:341–348. https://doi.org/10.1002/wmts.32

Fountain, S.J., and R.A. North. 2006. A C-terminal lysine that controls human P2X4 receptor desensitization. *J. Biol. Chem.* 281:15044–15049. https://doi.org/10.1074/jbc.M600442200

Garcia-Guzman, M., F. Soto, J.M. Gomez-Hernandez, P.E. Lund, and W. Stühmer. 1997. Characterization of recombinant human P2X4 receptor reveals pharmacological differences to the rat homologue. *Mol. Pharmacol.* 51:109–118. https://doi.org/10.1124/mol.51.1.109

Gonzales, E.B., T. Kawate, and E. Gouaux. 2009. Pore architecture and ion sites in acid-sensing ion channels and P2X receptors. *Nature.* 460:599–604. https://doi.org/10.1038/nature08218

Habermacher, C., K. Dunning, T. Chataigneau, and T. Grutter. 2016. Molecular structure and function of P2X receptors. *Neuropharmacology.* 104:18–30. https://doi.org/10.1016/j.neuropharm.2015.07.032

Haerteis, S., B. Krueger, C. Korbmacher, and R. Rauh. 2009. The delta-subunit of the epithelial sodium channel (ENaC) enhances channel activity and alters proteolytic ENaC activation. *J. Biol. Chem.* 284:29024–29040. https://doi.org/10.1074/jbc.M109.018945

Hattori, M., and E. Gouaux. 2012. Molecular mechanism of ATP binding and ion channel activation in P2X receptors. *Nature.* 485:207–212. https://doi.org/10.1038/nature11010

Helenius, A., and K. Simons. 1975. Solubilization of membranes by detergents. *Biochim. Biophys. Acta.* 415:29–79. https://doi.org/10.1016/0304-4157(75)90016-7

Ilyaskin, A.V., A. Diakov, C. Korbmacher, and S. Haerteis. 2016. Activation of the human epithelial sodium channel (ENaC) by bile acids involves the degenerin site. *J. Biol. Chem.* 291:19835–19847. https://doi.org/10.1074/jbc.M116.726471

Ilyaskin, A.V., A. Diakov, C. Korbmacher, and S. Haerteis. 2017. Bile acids potentiate proton-activated currents in *Xenopus laevis* oocytes expressing human acid-sensing ion channel (ASIC1a). *Physiol. Rep.* 5:e13132. https://doi.org/10.14814/phy2.13132

Ilyaskin, A.V., S.A. Kirsch, R.A. Böckmann, H. Sticht, C. Korbmacher, S. Haerteis, and A. Diakov. 2018. The degenerin region of the human bile acid-sensitive ion channel (BASIC) is involved in channel inhibition by calcium and activation by bile acids. *Pflugers Arch.* 470:1087–1102. https://doi.org/10.1007/s00424-018-2142-z

Irwin, J.J., and B.K. Shoichet. 2005. ZINC—a free database of commercially available compounds for virtual screening. *J. Chem. Inf. Model.* 45:177–182. https://doi.org/10.1021/ci049714+

Jelínkova, I., V. Vávra, M. Jindrichova, T. Obsil, H.W. Zemkova, H. Zemkova, and S.S. Stojilkovic. 2008. Identification of P2X(4) receptor transmembrane residues contributing to channel gating and interaction with ivermectin. *Pflugers Arch.* 456:939–950. https://doi.org/10.1007/s00424-008-0450-4

Kaczmarek-Hájek, K., E. Lörinczi, R. Hausmann, and A. Nicke. 2012. Molecular and functional properties of P2X receptors—recent progress and persisting challenges. *Purinergic Signal.* 8:375–417. https://doi.org/10.1007/s11302-012-9314-7

Kawate, T., J.C. Michel, W.T. Birdsong, and E. Gouaux. 2009. Crystal structure of the ATP-gated P2X(4) ion channel in the closed state. *Nature.* 460:592–598. https://doi.org/10.1038/nature08198

Khakh, B.S., and R.A. North. 2006. P2X receptors as cell-surface ATP sensors in health and disease. *Nature.* 442:527–532. https://doi.org/10.1038/nature04886

Latapiat, V., F.E. Rodríguez, F. Godoy, F.A. Montenegro, N.P. Barrera, and J.P. Huidobro-Toro. 2017. P2X4 receptor *in silico* and electrophysiological approaches reveal insights of ivermectin and zinc allosteric modulation. *Front. Pharmacol.* 8:918. https://doi.org/10.3389/fphar.2017.00918

Lefèvre, C.M., A. Diakov, S. Haerteis, C. Korbmacher, S. Gründer, and D. Wiemuth. 2014. Pharmacological and electrophysiological characterization of the human bile acid-sensitive ion channel (hBASIC). *Pflugers Arch.* 466:253–263. https://doi.org/10.1007/s00424-013-1310-4

Lennon, G., C. Auffray, M. Polymeropoulos, and M.B. Soares. 1996. The I.M.A.G.E. Consortium: an integrated molecular analysis of genomes and their expression. *Genomics.* 33:151–152. https://doi.org/10.1006/geno.1996.0177

Lorenz, C., M. Pusch, and T.J. Jentsch. 1996. Heteromultimeric CLC chloride channels with novel properties. *Proc. Natl. Acad. Sci. USA.* 93:13362–13366. https://doi.org/10.1073/pnas.93.23.13362

Morris, G.M., R. Huey, W. Lindstrom, M.F. Sanner, R.K. Belew, D.S. Goodsell, and A.J. Olson. 2009. AutoDock4 and AutoDockTools4: Automated docking with selective receptor flexibility. *J. Comput. Chem.* 30:2785–2791. https://doi.org/10.1002/jcc.21256

Negulyaev, Y.A., and F. Markwardt. 2000. Block by extracellular Mg^{2+} of single human purinergic P2X4 receptor channels expressed in human embryonic kidney cells. *Neurosci. Lett.* 279:165–168. https://doi.org/10.1016/S0304-3940(99)00976-3

North, R.A. 2002. Molecular physiology of P2X receptors. *Physiol. Rev.* 82:1013–1067. https://doi.org/10.1152/physrev.00015.2002

Popova, M., J. Trudell, K. Li, R. Alkana, D. Davies, and L. Asatryan. 2013. Tryptophan 46 is a site for ethanol and ivermectin action in P2X4 receptors. *Purinergic Signal.* 9:621–632. https://doi.org/10.1007/s11302-013-9373-4

Priel, A., and S.D. Silberberg. 2004. Mechanism of ivermectin facilitation of human P2X4 receptor channels. *J. Gen. Physiol.* 123:281–293. https://doi.org/10.1085/jgp.200308986

Sali, A., and T.L. Blundell. 1993. Comparative protein modelling by satisfaction of spatial restraints. *J. Mol. Biol.* 234:779–815. https://doi.org/10.1006/jmbi.1993.1626

Samways, D.S., B.S. Khakh, S. Dutertre, and T.M. Egan. 2011. Preferential use of unobstructed lateral portals as the access route to the pore of human ATP-gated ion channels (P2X receptors). *Proc. Natl. Acad. Sci. USA.* 108:13800–13805. https://doi.org/10.1073/pnas.1017550108

Samways, D.S., B.S. Khakh, and T.M. Egan. 2012. Allosteric modulation of Ca^{2+} flux in ligand-gated cation channel (P2X4) by actions on lateral portals. *J. Biol. Chem.* 287:7594–7602. https://doi.org/10.1074/jbc.M111.322461

Sanner, M.F. 1999. Python: A programming language for software integration and development. *J. Mol. Graph. Model.* 17:57–61.

Schmidt, A., R.J. Alsop, R. Rimal, P. Lenzig, S. Joussen, N.N. Gervasi, A. Khondker, S. Gründer, M.C. Rheinstädter, and D. Wiemuth. 2018. Modulation of DEG/ENaCs by amphiphiles suggests sensitivity to membrane alterations. *Biophys. J.* 114:1321–1335. https://doi.org/10.1016/j.bpj.2018.01.028

Sigworth, F.J., and S.M. Sine. 1987. Data transformations for improved display and fitting of single-channel dwell time histograms. *Biophys. J.* 52:1047–1054. https://doi.org/10.1016/S0006-3495(87)83298-8

Silberberg, S.D., M. Li, and K.J. Swartz. 2007. Ivermectin interaction with transmembrane helices reveals widespread rearrangements during opening of P2X receptor channels. *Neuron.* 54:263–274. https://doi.org/10.1016/j.neuron.2007.03.020

Tabibian, J.H., A.I. Masyuk, T.V. Masyuk, S.P. O'Hara, and N.F. LaRusso. 2013. Physiology of cholangiocytes. *Compr. Physiol.* 3:541–565. https://doi.org/10.1002/cphy.c120019

Trott, O., and A.J. Olson. 2010. AutoDock Vina: Improving the speed and accuracy of docking with a new scoring function, efficient optimization, and multithreading. *J. Comput. Chem.* 31:455–461. https://doi.org/10.1002/jcc.21334

Webb, B., and A. Sali. 2014. Comparative protein structure modeling using MODELLER. *Curr. Protoc. Bioinformatics.* 47:5.6.1–32.